*Quart. J. R. Met. Soc.* (1985), **111**, pp. 1087–1112 551.465.75:551.466.3

# A shallow water intercomparison of three numerical wave prediction models (SWIM)

By the SWIM Group: E. BOUWS[1], J. J. EPHRAUMS[2], J. A. EWING[3], P. E. FRANCIS[2], H. GUNTHER[4], P. A. E. M. JANSSEN[1], G. J. KOMEN[1], W. ROSENTHAL[4] and W. J. P. de VOOGT[5]

1. *Royal Netherlands Meteorological Institute, KNMI, De Bilt, The Netherlands*
2. *Meteorological Office, Bracknell*
3. *Institute of Oceanographic Sciences, Wormley*
4. *Institut fur Meereskunde and Max-Planck-Institut fur Meteorologie, Hamburg, F.R.G.*
5. *Delft Hydraulics Laboratory, Delft, The Netherlands*

(Received 18 July 1984; revised 10 June 1985)

SUMMARY

Three operational shallow water wave models are intercompared for two artificial experiments and verified for a severe storm hindcast, with the objectives of further understanding the effects of the parametrization of shallow water wave processes in numerical models.

The models used are the HYPAS (Max-Planck Institute) and GONO (KNMI) coupled-hybrid models, and the BMO (Meteorological Office) coupled-discrete model which are all briefly described. In the first case, depth-dependent fetch-limited wave growth in a steady wind is examined. In the second case a steady onshore wind is specified over an idealized constant slope coastal shelf, and the stationary wave spectra at various depths are intercompared. For the third case the wind fields for the North Sea storms of 18–26 November 1981 were accurately reconstructed and used by each model in its operational configuration to produce a wave hindcast for this period.

In case 1 the GONO and BMO models exhibit similar behaviour in the evolution of energy and peak frequency, whereas HYPAS displays less depth attenuation and little variation in peak frequency. In case 2 the energy values at different shelf depths are approximately as predicted in case 1 for HYPAS though rather higher for BMO and GONO. However, GONO and HYPAS show little change in peak frequency with depth here whereas BMO wave spectra become double-peaked with a wind-sea peak migrating to higher frequencies in shallower waters. In case 3, the hindcasts, all models produce qualitatively similar results. The time series of wave height and period agree well with measurements, BMO and HYPAS predicting correct energy levels except at storm peaks and GONO generally overpredicting both at lower energy levels and in a duration-limited strong wind case. The r.m.s. error in wave height at the southern shallow water verification site is 0·5 m for all models, and varies between 0·9 m (GONO) and 1·5 m (HYPAS) at the northern deep water site. Some wave spectra are presented and the directional relaxation of wind-sea in each model is illustrated.

The results of cases 1 and 2 are readily explained by the formulation of shallow water processes adopted in each model, but it is difficult to isolate and identify these mechanisms in the measured or modelled spectra from the hindcast. It is suggested that future studies involving detailed verification and intercomparison of wave models should be confined to more carefully designed wave-measuring experiments so that less ambiguous results are obtained.

## 1. INTRODUCTION

In this paper we intercompare three numerical wave prediction models, which are used for wave prediction in depth-limited situations. The models are the British Meteorological Office model, BMO (Golding 1983); GONO (GOlven NOrdzee) which is in use in the Netherlands (Janssen *et al.* 1984) and HYPAS (HYbrid–PArametric–Shallow) which was developed by a group in Hamburg (Gunther and Rosenthal 1984).

All three models are in operational use for the prediction of sea state in areas in which depth limitations to the wave height can be important, such as the North Sea.

The present study can be seen as a follow-up to the Sea Wave Modelling Project (SWAMP 1982, 1985). In SWAMP ten numerical wave prediction models were studied. The models were run on artificial wind fields and for simplified geometries. The cases were constructed so as to bring out differences between the models in as clear a manner as possible. SWAMP was successful because it gave considerable insight into the behaviour of the models. Strong and weak points were identified, and also valuable suggestions emerged about points to be clarified. SWAMP was concerned with deep water waves only; shallow water aspects of the models were not studied. Depth limitations

are, however, of great significance in practical applications concerning offshore constructions and coastal protection. Typically, extreme storms generate significant wave heights in the southern North Sea (depth ~30 m) that are only half as large as in the deeper central part. This sizable energy reduction occurs because the dispersion relation is already sensitive to the depth, and energy dissipation by bottom effects can be important. In our models we concentrate on these mild shallow water effects. We exclude situations of extreme shallow water where bottom-induced nonlinear effects, such as wave breaking, are significant for the energy balance. Our study is concerned with processes well outside the surf zone, where wave heights do not reach the same order of magnitude as the local water depth.

This study was undertaken to improve an understanding of depth-related effects as represented in numerical wave models. As in SWAMP we compared our models in idealized situations, which were now chosen to highlight shallow water features of the models. The study of artificial cases has the advantage that one can focus on a special aspect of model performance, in contrast to realistic situations which normally exhibit the mixed results of many different processes, such as varying depth, irregular coastlines and non-uniform winds and currents. This selectivity allows us to study the different physical concepts in the models and their numerical realizations. Furthermore we can clarify points where additional theoretical or experimental work is needed.

We decided also to make a realistic hindcast, using the same wind fields in each model, and to compare with available field data to see how our models perform under these more complicated conditions. In this respect the present work is a continuation of earlier operational intercomparisons (Bouws *et al.* 1985b; Gunther *et al.* 1984). Those comparisons were, however, based on operational results in which the models were driven by real-time analysed wind fields. The model results thus always depend rather strongly on the quality of the wind fields, the accuracy of which have been improved in the current study. In the case of Bouws *et al.* different wind fields were used in the different wave models which further complicated the analysis of results.

A good summary of our present knowledge of deep water aspects of wave modelling can be found in the SWAMP report (SWAMP 1985). There it is explained how an interplay between wave generation, nonlinear interactions, dissipation and whitecapping leads to the observed quasi-universal spectral shape of wind-waves and the slow evolution of the characteristic features of the spectrum such as total energy, and peak frequency. Wave modelling in finite depths has recently been reviewed by Vincent (1982). The most direct transition from deep water to shallow water modelling is by means of an additional term in the energy balance equation which represents the energy dissipation by the bottom. The possible mechanisms that might contribute to this dissipation are discussed in a paper by Shemdin *et al.* (1978) where further references may be found. The dissipation rate is typically modelled to be linear in the energy density. This has been observed most clearly for nearly monochromatic swell on finite depth water (Hasselmann *et al.* 1973).

This direct method of modelling bottom dissipation is used in all three models for the description of swell propagation when the atmospheric input and the nonlinear interaction between different frequency–direction bands are negligible. Interesting differences between the models appear in our approach for that part of the spectrum where atmospheric input and nonlinear interaction are not small. We will discuss these differences in the course of this paper.

The plan of the paper is as follows. In section 2 we summarize the most important features of our models, with emphasis on shallow water aspects. The third section describes results from runs with idealized wind fields. We consider two cases: fetch- and duration-limited wave growth over a flat finite-depth bottom, and growth over the

frequently occurring situation of a linearly sloping bottom. Section 4 discusses our hindcast of a storm which occurred in November 1981; it gives model results, a discussion of field data and a comparison both between models and between models and data. Section 5 summarizes our conclusions.

## 2. Review of the three models

The evolution of a surface gravity wave field in space and time is determined by the balance equation for the action density, $N$,

$$\partial N/\partial t + (\partial \omega/\partial \mathbf{k})\cdot(\partial N/\partial \mathbf{x}) - (\partial \omega/\partial \mathbf{x}) \cdot (\partial N/\partial \mathbf{k}) = S = S_{\text{in}} + S_{\text{nl}} + S_{\text{ds}} + S_{\text{b}} \qquad (1)$$

where $N = F/\sigma$, $F(\mathbf{k}, \mathbf{x}, t)$ is the two-dimensional surface wave (variance) spectrum, which depends on wavenumber vector $\mathbf{k}$ (or frequency $f$ and direction $\theta$) and position $\mathbf{x}$; $\omega = \sigma + \mathbf{k}\cdot\mathbf{U}$ (where $\mathbf{U}$ is the slowly varying current), $k = |\mathbf{k}|$ and $\sigma(k) = (gk \tanh kD)^{1/2}$ ($D$ is depth) is the dispersion relation for surface gravity waves. The net source function $S$ is represented as the sum of the input $S_{\text{in}}$ by wind, the nonlinear transfer $S_{\text{nl}}$ by resonant four-wave interactions, the dissipation $S_{\text{ds}}$ by e.g. whitecapping and the dissipation $S_{\text{b}}$ by e.g. bottom friction. In this study we shall confine ourselves to cases where the effect of the current $\mathbf{U}$ can be neglected so that $\omega = \sigma$. Using this approximation Eq. (1) becomes for the frequency spectrum $F(f, \theta, \mathbf{x}, t)$

$$\partial F/\partial t + \nabla\cdot(\mathbf{c}_{\text{g}}F) - \partial(RF|\mathbf{c}_{\text{g}} \wedge \nabla D|)/\partial\theta = S \qquad (2)$$

where $R = k/(\sinh kD \cosh kD + kD)$, $\mathbf{c}_{\text{g}} = \partial\omega/\partial\mathbf{k}$, and $S$ is newly defined in frequency space. The derivation of Eq. (2) from Eq. (1) is given in the appendix.

All models in this study attempt to compute the two-dimensional wave spectrum by numerical integration of (2) or an approximation of (2). The models BMO, GONO and HYPAS differ on the one hand in the form assumed for the source function $S$ and on the other hand in the treatment of wind-sea. This difference in wave modelling was also recognized by the SWAMP study (1985) on deep water where modern wave models were divided into two classes, namely the coupled discrete spectral (C.D.) models and the coupled hybrid (C.H.) models. The BMO model belongs to the first class and uses for the prediction algorithm discrete frequency and direction intervals and the energy content in these intervals is predicted. The GONO and HYPAS models belong to the second class. These models use only discrete frequency and direction intervals for the calculation of swell, whereas the wind-sea part of the spectrum is parametrized by a number of prognostic variables such as the peak frequency and Phillips constant that determine the shape of the wind-sea spectrum. In SWAMP (1982, 1985) it was shown that both types of models are capable of realistically modelling the behaviour of the sea state, although a delicate point is the separation between wind-sea and swell. In the remainder of this section we summarize the properties of the models with emphasis on the algorithms for modelling finite depth effects.

### (a) *BMO model*

This model is described by Golding (1983), and in the SWAMP study (1982, 1985) its results for artificial wind fields are compared with those of other models, such as GONO and HYPAS. The propagation of wave energy at all frequencies is performed using an accurate form of a Lax–Wendroff scheme. The wind input term is given by the combined Phillips–Miles growth term,

$$S_{\text{in}} = \alpha + \beta F \qquad (3)$$

where $\alpha$ and $\beta$ depend on frequency, wind speed $u_{19.5}$ (at 19·5 m) and direction. The dissipation by whitecapping is assumed to be given by

$$S_{ds} = -\delta f^2 E^{1/4} F \tag{4}$$

where $\delta = 3\times10^{-4}$ and where $E = \int F df d\theta$ is the total energy. For finite water depth there is an additional dissipation by bottom friction (Collins 1972):

$$S_b = \phi_1 g k^2/(2\pi f \cosh kD)^2 \langle U\rangle F, \tag{5}$$

where $\langle U\rangle = \{\int (gk/2\pi f \cosh kD)^2 F df d\theta\}^{1/2}$ and $\phi_1 = 0{\cdot}015$. The effect of the nonlinear interactions is achieved by reshaping the wind-sea spectrum after all these processes into a JONSWAP spectrum (Hasselmann *et al.* 1973), the peak frequency $f_p$ and shape parameters $\gamma$ and $\alpha$ of which follow from the deep water, diagnostic, relations with the total wind-sea energy $E_w$. $E_w$ is initially integrated in the domain of $f > 0{\cdot}8 f_{pM}$, $|\theta-\phi|<90°$, where $f_{pM} = g/(2\pi u_{19.5})$ is the Pierson–Moskowitz frequency and $\phi$ the local wind direction. Having positioned the peak of the new wind-sea spectrum at $f_p$ a check is made to ensure that all energy at $f > 0{\cdot}8 f_{pM}$ has been conserved and that energy in the range $0{\cdot}8 f_{pM} < f < 0{\cdot}8 f_p$ has been undisturbed. This procedure retains the separate identity of swell at $f < 0{\cdot}8 f_p$ in most situations.

### (*b*) *GONO model*

A detailed description of GONO may be found in Janssen *et al.* (1984). GONO is a coupled-hybrid model which for the prediction of wind-sea uses the total wind-sea energy and the average direction as prognostic variables. The other spectral parameters, such as the peak frequency, are given by diagnostic relations, which are supposed to be the same in deep and shallow water.

The wind-sea spectrum in GONO differs slightly from the JONSWAP shape used in the BMO, and the TMA spectrum used in the HYPAS model, as will be seen in section 3. For wind-sea the averaged energy balance equation

$$\partial E/\partial t + \nabla\langle c_g\rangle E = \langle S\rangle = \langle S_{in}\rangle + \langle S_{ds}\rangle + \langle S_b\rangle \tag{6}$$

is solved, where $\langle c_g\rangle$ is the average group velocity and $\langle S\rangle$ is the total energy source term averaged over frequency and direction. The advection term is determined by means of an energy-conserving, first-order, upwind scheme. The combined effect of wind input and dissipation by whitecapping is determined by observations at infinite fetch. Bottom dissipation is expressed as

$$\langle S_b\rangle = (-\Gamma/g^2) \int (\omega/\sinh kD)^2 F df d\theta \tag{7}$$

where $\Gamma = 0{\cdot}027\,\mathrm{m^2 s^{-3}}$. In this fashion the wind-sea energy is determined at every grid point.

The calculation of the wave energy (which is the sum of wind-sea energy and swell) is done for a number of output points only. The swell energy is propagated along rays and the method of combining wind-sea and swell is essentially that at the output points for every frequency band and directional sector the maximum is taken of the advected energy in the rays and the local wind-sea.

### (*c*) *The HYPAS model*

The deep water part of the model is discussed in Gunther *et al.* (1979). The model combines the traditional approach of independent calculation of swell energy for each frequency and direction band through a ray technique, with a parametrical wind-wave

model, using the parameters of the JONSWAP spectrum and the mean wind-sea direction as prognostic variables. Wave energy in the frequency range below that of the local wind-sea spectrum is processed by means of the ray technique, the discrete spectral part of the modelling process.

For shallow water the conventional concept of adding a bottom dissipation term $S_b$ to the deep water source terms has been abandoned. For a full description of the physical assumption, the mathematical algorithms and the numerical realization we refer to a paper by Gunther and Rosenthal (1984). The foundation for HYPAS was laid by experimental evidence that wind-waves in shallow water exhibit a universal spectral shape (the TMA spectrum) that is depth dependent (Bouws *et al.* 1985a). The TMA shape passes over to the JONSWAP shape for increasing water depth and the characteristic parameters of the TMA spectrum are chosen to be the same as the JONSWAP parameters for deep water.

The TMA shape coincides for the high frequency side with results of Kitaigorodskii *et al.* (1975). The explanation given by these authors is a hypothetical saturation range extending over a certain frequency range where energy is transferred to higher frequencies without dissipation. Due to the limited range of such a saturation range this hypothesis cannot explain the TMA shape.

Instead of the assumptions made by Kitaigorodskii *et al.*, HYPAS uses the concept that the shape of a spectrum with fixed peak frequency is mainly determined by the balance of three source terms:

$$S_{in} + S_{nl} + S_{ds} = 0. \tag{8}$$

Depending on water depth this balance determines the depth dependence of the TMA spectrum. Since the field data indicate that there is no dependence on bottom parameters (e.g. grain size) it is assumed that for a given frequency the dissipation mechanism $S_{ds}$, present already in deep water, varies monotonically with wave number $|\mathbf{k}|$ and causes the dependence of the TMA shape on water depth.

The time and spatial development of the peak frequency and the shape parameters $\alpha$ and $\gamma$ of the JONSWAP spectrum, and the mean wind-sea direction, is modelled similarly to that in deep water. For shallow water, diagnostic relations between the spectral parameters are used, which differ from the deep water ones. For the cases studied so far with HYPAS there has been no reason to include the direct influence of bottom effects as discussed by Shemdin *et al.* (1978) or to include a depth limitation of wave growth that has been postulated in the literature (Bretschneider 1958).

## 3. IDEALIZED CASES

### (a) *Case I, results*

In this case we study ideal generation by a constant off-shore wind (see Fig. 1). The wind speed is taken to be $20\,m\,s^{-1}$. For the bottom depth we have chosen $D = 15, 30, 60$ and $120\,m$. This case was selected because it allows us to study the effect of depth limitation in a simple context. In all three models the bottom influence leads to a frequency-dependent reduction of spectral level. As discussed in the previous section the resulting shallow water spectra differ from the corresponding deep water ones. It is useful to characterize these differences by studying the behaviour of the total energy and the peak frequency, both as a function of fetch and duration. In Fig. 2 we have plotted the non-dimensional wave energy $E_*$ as a function of non-dimensional fetch, $X_*$. These non-dimensional quantities are defined as $X_* = Xg/u_*^2$, $E_* = Eg^2/u_*^4$.

As in SWAMP (1982, 1985) we scaled with the friction velocity, $u_*$, because $u_*$ is

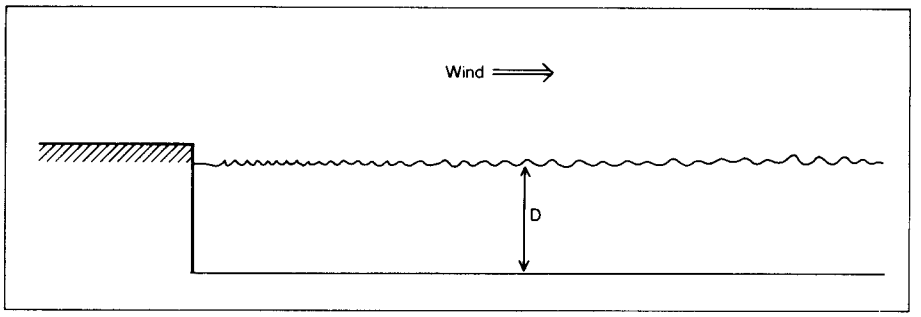


Figure 1. Configuration of case I: a constant off-shore wind blowing over a basin of constant depth $D$.

supposed to characterize the turbulent boundary layer better than the wind speed at a given height. We have taken $u_* = C_D^{1/2} u_{10}$ with $C_D = 1{\cdot}83 \times 10^{-3}$ for $u_{10} = 20\,\mathrm{m\,s^{-1}}$. For convenience we have also indicated $E$ and $X$. The results of Fig. 2 were obtained by starting from a flat sea at $t = 0$, and by running the models until they became stationary. For a depth of 120 m the growth curves are effectively deep water curves. These deep water curves have already been discussed in the SWAMP report. From Fig. 2 one notes that BMO and HYPAS behave very similarly for deep water. GONO reaches approximately the same asymptotic level, but more slowly, whereas for short fetches it has higher energy values than the other models. The most striking feature of Fig. 2 is

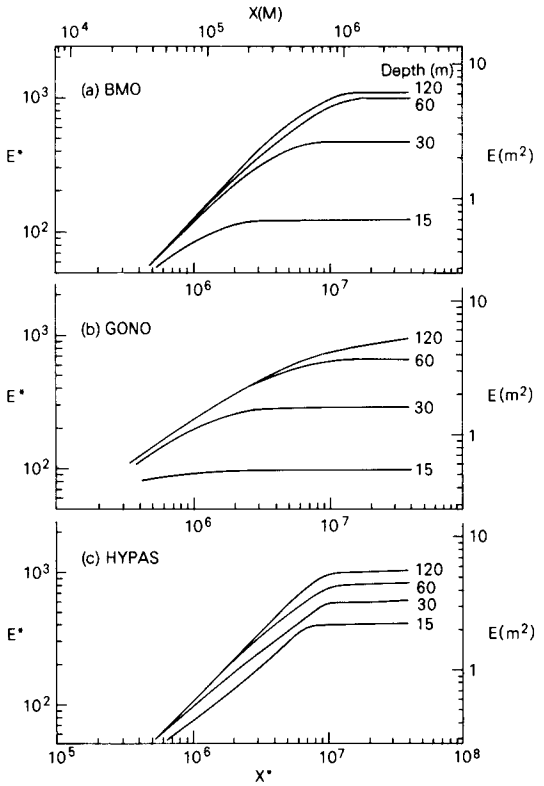


Figure 2. Plots of wave energy $E(\mathrm{m}^2)$ and non-dimensional energy $E_*$ against fetch $X(\mathrm{m})$ and non-dimensional fetch $X_*$ in the depth-dependent ($D$ = 120, 60, 30, 15 m) fetch-limited configuration of case I from the three models (a) BMO, (b) GONO, (c) HYPAS.

the reduction of wave energy $E_\infty$ in the fully grown state due to bottom effects. The reduction is relatively weak in HYPAS ($E_\infty$HYPAS(120) = 5·5 m$^2$, $E_\infty$HYPAS(15) = 2 m$^2$) and rather strong in GONO ($E_\infty$GONO(15) = 0·4 m$^2$) and BMO. In Fig. 3 we have indicated the dimensionless peak frequency $f_p^* = f_p u_*/g$ as a function of $X_*$. This figure also emphasizes the difference between BMO and GONO on the one hand, and HYPAS on the other hand. In BMO and GONO the peak frequency in the asymptotic steady state is much higher in shallow water than in deep water. In HYPAS the peak frequency does not vary much with depth. This should not be surprising after our discussion in section 2. Indeed, the differences in model behaviour can be related directly to the physical ideas behind the parametrization of the depth influence. In HYPAS enhanced whitecapping and/or turbulent diffusion reduces the spectral energy level over the full spectral range, and this leads to a reduction of wave energy but it does not affect the peak frequency very much. The other models have strongest bottom effects for long waves, which leads to both an energy reduction and a shift in peak frequency. A comparison of the duration-limited growth curves (not reproduced here) led to similar conclusions. The situation is summarized in Fig. 4 where we show the asymptotic spectra for each of the models (infinite fetch and infinite duration) as a function of depth.

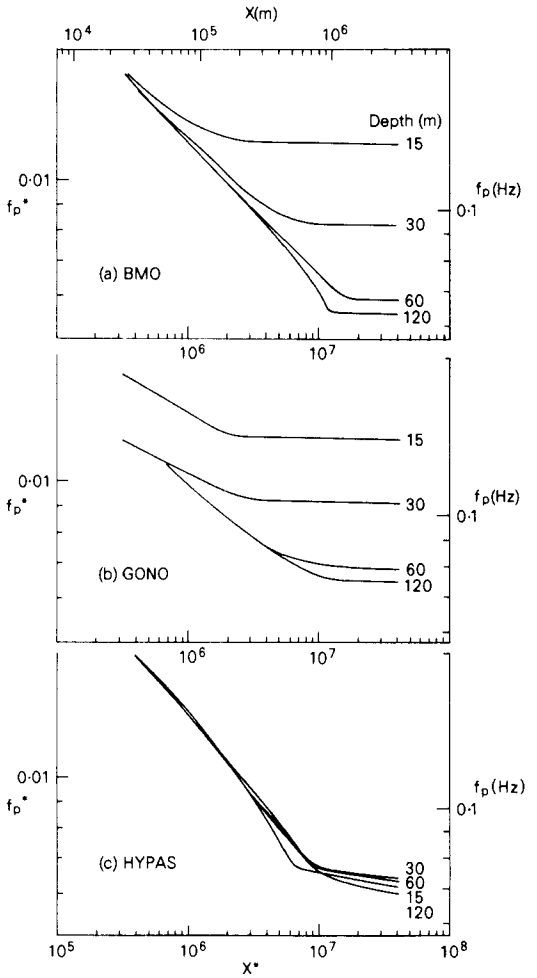


Figure 3. Plots of peak frequency $f_p$ (Hz) and non-dimensional peak frequency $f_{p*}$. As Fig. 2.

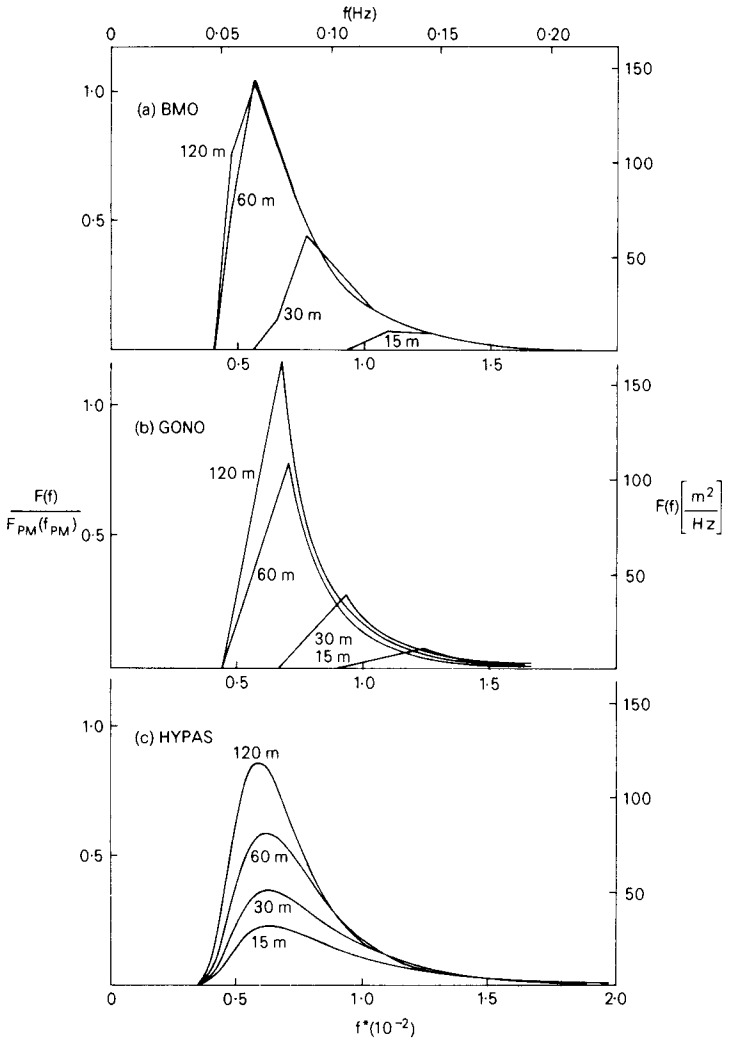


Figure 4. The fully developed wave energy spectra as a function of depth ($D$ = 120, 60, 30, 15 m) from the three models (a) BMO, (b) GONO, (c) HYPAS, for case I. The wave energy density $F(f)$ (m$^2$/Hz) is plotted against frequency $f$(Hz) and non-dimensional frequency $f_* = fu_*/g$. Also shown is the energy density scaled by the peak energy density of the Pierson–Moskowitz spectrum $F_{PM}(f_{PM}) = Af^{-5}\exp\{-B(f_{PM}/f)^4\}$, $A = 5 \times 10^{-4}$, $B = 1{\cdot}25$, $f_{PM} = 0{\cdot}13\ g/u_{10}$.

## (*b*) *Case I, discussion*

It is desirable to trace back the marked differences in model behaviour to differences in the algorithms used for integrations of the energy balance equations. These algorithms differ because they rely on different assumptions about the source terms.

The behaviour of GONO and BMO in case I originates from the explicit energy sink which limits wave growth and leads to a depth-dependent saturation value for the wave height. Use of the deep water diagnostic relationship between $f_p$ and $E$ automatically leads to an increase of $f_p$ with decreasing depth.

Despite the fact that HYPAS does not have an explicit extra dissipation term, the qualitative behaviour of the growth curve (limited wave growth and depth-dependent saturation value) is similar to that of BMO and GONO. However, the differences in

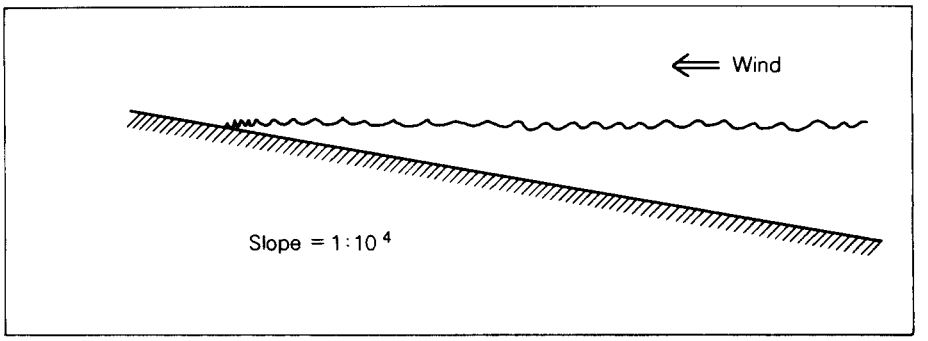


Figure 5. Configuration of case II: a constant onshore wind blowing over an idealized sloping coastal shelf.

approach become apparent in the behaviour of the peak frequency. HYPAS uses the peak frequency $f_p$ as one of the prognostic variables. The fetch behaviour of that parameter is very similar to the well-known deep water law; however, the wavenumber connected with $f_p$ is depth dependent. The dissipation mechanism (being present in deep and shallow water) is assumed to depend on wavenumber, and therefore the total energy for the same $f_p$ is decreasing with decreasing water depth.

### (c) *Case II, results*

Here we investigate wave evolution by a constant wind field over a sloping bottom. The geometry is depicted in Fig. 5. Wind is blowing towards shore with a speed of $20\,m\,s^{-1}$. The bottom was chosen to rise linearly with a slope of $1{:}10^4$. This slope is typical for the southern North Sea. Case II was selected as an idealization of situations encountered frequently in coastal areas. As in case I the models start from a flat sea, and are run until a stationary state has been reached, with the fully developed deep water spectrum as a boundary condition. We analysed this stationary solution only.

The very different outcomes for the three models are shown in Figs. 6, 7 and 8. In Fig. 6 the dimensionless energy is given as a function of $X_* = Xg/u_*^2$, with $X$ now representing the distance to shore. All models show a reduction in wave energy, from maximum values of wave height in deep water of about 9·5 m to values around 5·5 m in a depth of 20 m. BMO has the strongest attenuation rate for depths of less than 20 m while HYPAS has the weakest rate. For the HYPAS model the wave heights at a given depth are similar to the saturation values obtained for the same depth in case I. However, for BMO and GONO wave heights are greater than the corresponding saturation values in case I, the margin increasing with decreasing depth for GONO and having a maximum at about 30 m depth in BMO.

The peak frequencies are given in Fig. 7. The behaviours of GONO and HYPAS are very similar, both models exhibit a peak frequency that does not deviate much from the deep water value. In contrast the BMO result shows a strong increase of peak frequency with decreasing depth. All models have a local peak frequency which is lower than the saturation peak frequency at the same depth exhibited in case I.

Figure 8 represents the wave spectra for different depths, given sufficient fetch and duration to reach equilibrium conditions. The earlier discussion concerning the behaviour of peak frequency and total energy can be extended to these figures in a straightforward manner. The double peak in the BMO spectra for shallow depths is discussed below; the peak frequency used in the preceding discussion is defined as the higher frequency when there is a double peak.

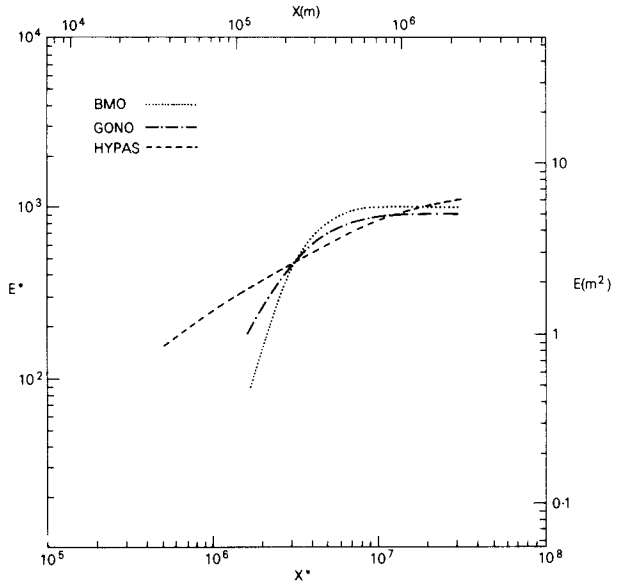


Figure 6. The stationary distribution of wave energy $E(\mathrm{m}^2)$ and non-dimensional wave energy $E_*$ as a function of distance $X$(m) and non-dimensional distance to shore from the three models for case II. Depth in metres is $D = X/10^4$.

### (*d*) *Case II, discussion*

In case II the BMO model exhibits stronger dissipation than that of the other models in depths less than 20 m; however, wave heights at a given depth are higher than in case I. This is because of the advected energy from deep water, which is not present in case I and which is not entirely dissipated until very shallow water is reached, e.g. less than 15 m.

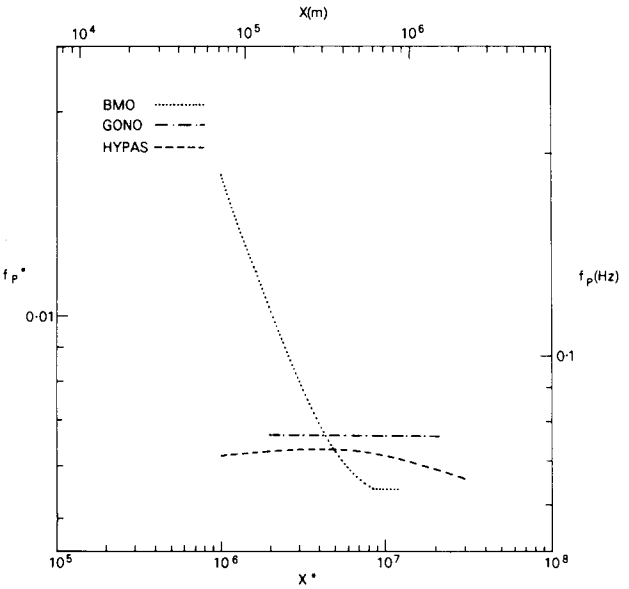


Figure 7. The stationary distribution of peak frequency $f_p$(Hz) and non-dimensional peak frequency $f_{p*}$ from the three models. As Fig. 6.

The origin of the double-peaked spectra in the BMO model in case II (Fig. 8) can be found in the procedure which locates the new wind-sea spectrum once other physical processes have been computed. In shallow water the dominant process is bottom dissipation, $S_b$. The resultant decrease in energy levels at all frequencies leads to an increase in $f_p$, since a deep water relationship between $f_p$ and the wind-sea energy is still applied. The wind-sea spectrum is then redefined and modelled at $f > 0{\cdot}8f_p$, whilst there still remains energy at lower frequencies which has propagated in from deeper water and is not completely dissipated.

In GONO, in case I, the sea state is computed in the parametric (wind-sea) part, and it is assumed that there is a local quasi-equilibrium between the source terms. In case II this quasi-equilibrium is disturbed, because energy propagates from the fully developed state in deep water into shallower regions. Therefore, GONO treats this case in the discrete spectral ('swell') part of the model. In this part only the dissipation source term $S_b$ is retained. The resulting equilibrium is the result of a local balance between advection divergence and bottom dissipation. This leads to an almost constant peak frequency and a decreasing total energy, which is, however, at a higher level than that of equilibrium in case I.

The results of HYPAS in this case originate from the use of $f_p$ as a prognostic variable. This equation for $f_p$, in the stationary state, has the form

$$c_g(f_p)(\partial f_p/\partial x) = S_f(f_p)$$

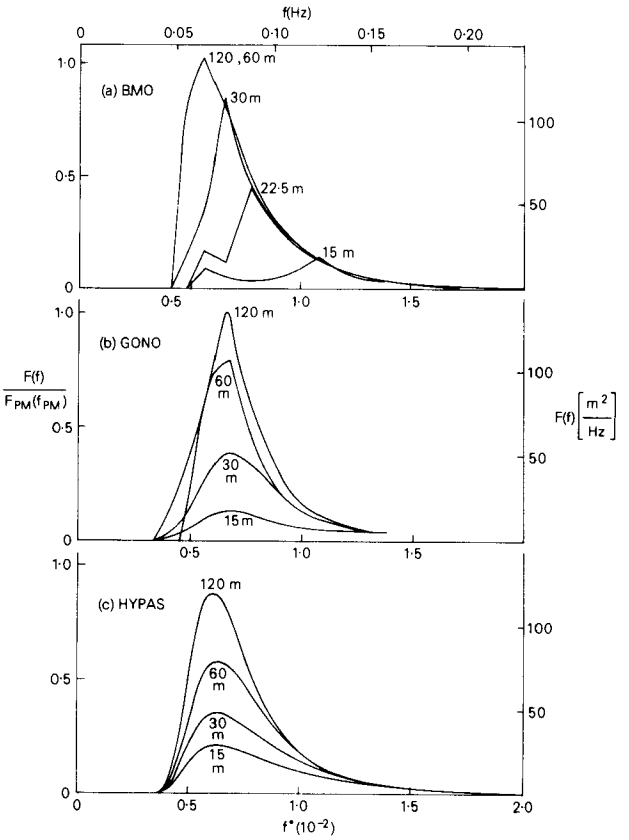


Figure 8. The stationary wave energy spectra as a function of shelf depth from the three models (a) BMO, (b) GONO, (c) HYPAS for case II. As Fig. 4.

if the small coupling terms to the other parameters are neglected. It can be seen directly that the function $f(x) = f_{pM}$ is a solution to this equation, satisfying the correct boundary value in deep water, because by construction $S_f(f_{pM}) = 0$. The HYPAS behaviour in cases II and I is very similar. This can be understood because in HYPAS the assumption that locally an equilibrium exists requires a strong dissipation, nonlinear in the spectral energy density. In fact, it is quite possible to imagine a dissipation strong enough for this equilibrium to be the same in case I (no advection divergence) and case II (sizeable advection divergence). A very interesting fact is the apparent similarity of the GONO and HYPAS spectra. In GONO, the strong reduction of the energy at around 1·5 times the peak frequency is, especially at small fetch, due to bottom dissipation. In HYPAS it results from the wavenumber dependence of the whitecapping and/or viscous diffusion.

### (*e*) *General discussion of idealized cases*

The analysis of the idealized cases indicates the existence of a fair amount of uncertainty with respect to depth-limited wave modelling. This is partly due to a lack of reliable and uncontaminated observations, and partly to the unavailability of exact solutions of Eq. (2).

There is only limited experimental material available on which to base theories for wave growth in shallow water. Some of this evidence has been summarized by Holthuijsen (1980), and broadly speaking the behaviour of the GONO and BMO models in case I is supported by these data. However, details of the experiments imply some degree of doubt as to such important aspects as the consistency of the associated wind field, the definitions of peak frequency and the flatness of the sea bed.

Another major data set has been constructed from the results of the MARSEN experiment in 1979 and the ARSLOE experiment in 1980, together with a number of spectra from the so-called Texel storm in 1976. A total of about 3000 spectra have been collected to derive data for growing waves in water of finite depth (Bouws *et al.* 1985a). The HYPAS model has been developed from the evidence of this TMA (Texel–Marsen–Arsloe) data set. Again, there is some doubt as to the homogeneity of the collected data, in this instance advected energy from deeper water may be present in some of the spectra thus removing similarities with case I.

A problem with the theoretical construction of solutions of Eq. (2) is not only the complexity of the nonlinear transfer and the uncertainty about the dissipation source term, but also the delicacy of the balance between the various source terms in growing seas. Komen *et al.* (1984) found that in the steady state cancellation between different source terms gives a remainder that is smaller by two orders of magnitude. Bouws and Komen (1983) attempted the simulation of depth-limited wave growth. Their work included the full nonlinear transfer and an explicit bottom dissipation term. They were able to describe the balance in an extreme depth-limited storm provided they included advection from deep water, and they also found that the explicit bottom dissipation term was an important feature. However, one might doubt the uniqueness of this solution, since the HYPAS results of this study suggest that a solution based on Kitaigorodskii-scaling might also be possible.

## 4. Hindcast study of real storm events, case III

### (*a*) *Introduction*

Although the idealized cases studied in earlier sections allow us to isolate individual processes, the real test of any numerical simulation model is how well it represents the complex and interacting processes to be found in a real geophysical system. The three

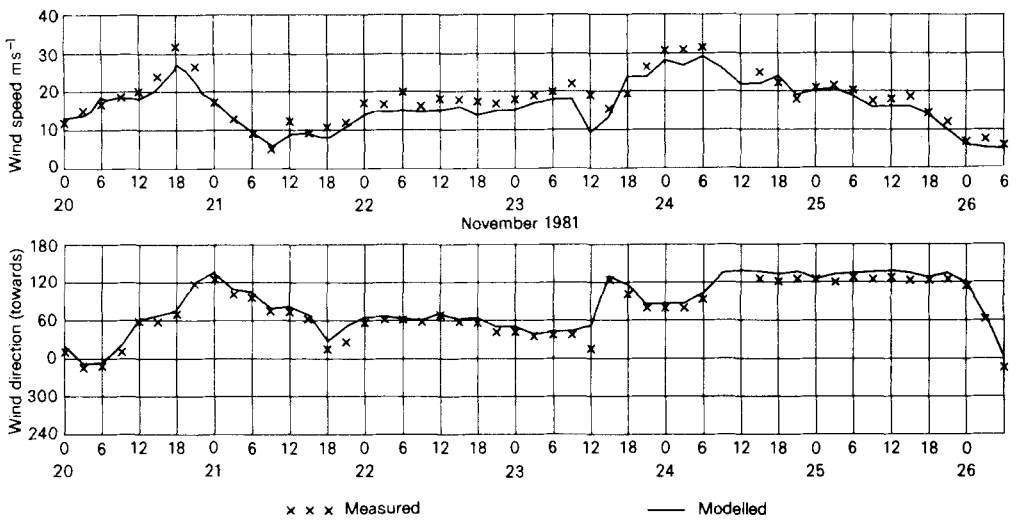


Figure 9. Measured (anemometer level 85m) wind speed and direction at Fulmar (56·4°N 2·1°E) during the hindcast period 20–26 November 1981 compared with the numerically reconstructed winds used by each wave model.

models discussed in this paper are all in use as forecasting aids for various services in European off-shore areas and were thus easily set up to run in hindcast mode using common wind fields. We hoped that the idealized cases (I and II) could be identified in a real situation and some parallels drawn as to model performance in both simple and complex conditions. How well that hope was realized, and how the models performed generally in a hindcast simulation of a real storm in shallow water is detailed in what follows. The storm event chosen, 20–26 November 1981, was selected as a result of two basic criteria: that sufficient reliable spectral wave measurements could be accessed; and that the relevant wind fields over a large enough area could be numerically analysed and reconstructed. At the time of the inception of this project (December 1982) the chosen storm was the one that was most rapidly identified as meeting both conditions outlined above.

### (*b*) *The meteorological situation*

The synoptic situation during the period of study, 20–26 November 1981, was dominated by the passage of two active low pressure areas. The first was a rapidly moving system which travelled from 15°W (NW of Ireland) to 10°E (over southern Norway) in the 24 hours from midnight on the 20th to midnight on the 21st. The associated surface wind fields, predominantly light and southerly initially, grew progressively stronger, and veered, throughout the course of the day over central and southern areas of the North Sea. The wind data measured at Fulmar (56·4°N 2·1°E) are shown in Fig. 9, where a maximum of around 30 m s$^{-1}$ can be seen at 18 z on the 20th, coming from WSW. Further to the south and east at FPN (54·7°N 7·2°E) the peak of the storm occurred six hours later when a maximum of nearly 25 m s$^{-1}$, from a more westerly direction, was measured. The synoptic situation on the 20th is illustrated in Figs. 10(a) and (b). During the 21st and 22nd a weak ridge of high pressure was the dominant feature in the central and southern North Sea, with steady winds of 10–15 m s$^{-1}$ mainly from WSW.

A further low pressure area was stationary just north of Scotland during this time, which began to deepen towards the end of the 22nd. During the 23rd this second storm of interest began to deepen rapidly and also to move slowly eastward towards Scandinavia,

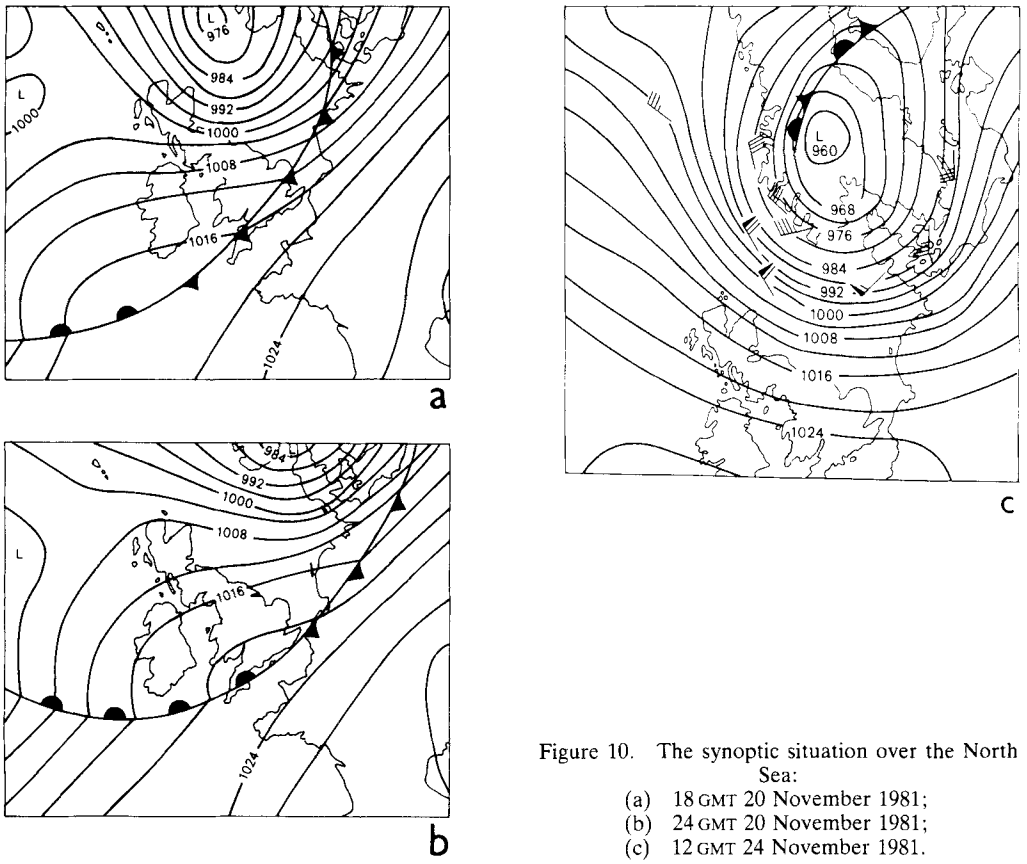


Figure 10. The synoptic situation over the North Sea:
(a) 18 GMT 20 November 1981;
(b) 24 GMT 20 November 1981;
(c) 12 GMT 24 November 1981.

an associated cold front moving gradually east and south during the day. The storm centre continued to move slowly eastward throughout the 24th, bringing most parts of the North Sea under the influence of northerly winds by 12 z. In Fig. 9 it can be seen that the strong winds ($\sim 30\,m\,s^{-1}$) were more sustained in this slower moving storm and associated with the passage of the cold front. Figure 10(c) illustrates a subjective analysis of the surface pressure pattern at the height of the second storm, with some of the observed wind information also plotted.

### (*c*) *Processing the wind data*

The numerical wind fields were derived by further processing of data originally obtained from the then operational numerical weather prediction model of the Meteorological Office (Burridge and Gadd 1977). That model produced forecast wind data, on a regular polar stereographic projection grid, at 900 mb at 3-hourly intervals for a 12-hour period. Employing empirical relationships between observed 900 mb and surface winds (Findlater *et al.* 1966), these data were then used to generate first guess surface wind fields. These fields were subsequently improved by means of numerical analysis routines which relaxed the field values towards those of the fairly dense network of observations which are available for the area of the continental shelf. The accuracy of the technique can be assessed from Fig. 9 and also by comparing Figs. 10(c) and 11. In Fig. 9 the observations are in an unreduced state, i.e. exactly as measured by the anemometer at a height of 85 m. The modelled winds are generally slightly less than those observed (at

TABLE 1. WAVE MODEL VALIDATION DATA

| Station | Position | Depth (m) | Wave recorder type | Length of record (min.) | Degrees of freedom | Source of data |
|---|---|---|---|---|---|---|
| Fulmar | 56·4°N 2·1°E | 80 | Wave staff and e.m. current meters | 60 | 60 | Shell Development Company, Houston |
| K-13 | 53·2°N 3·2°E | 28 | Waverider buoy | 20 | 24 | Rijkswaterstaat Netherlands |

this location) since the analysed wind fields are nominally those at a height of about 20 m. The overall match for direction and speed is very acceptable. A comparison of Fig. 10(c) and Fig. 11 shows the good areal match between the subjectively drawn surface pressure and the objectively analysed wind field. The very strong wind plotted at 60°N 2°E was almost certainly measured at a very high level. Other time series of observed and modelled winds are available which also confirm the high quality of the wind fields used in the wave hindcast calculations.

### (*d*) *The measured wave data*

We obtained measured wave data at seven stations in the North Sea which were used to compare with the predictions from the models. However, for reasons of space, we discuss in this paper the results from only two stations: the full set of comparisons will be reported elsewhere. Details of the two stations are given in Table 1. One station (Fulmar) is in deep water in the northern part of the North Sea, the other station (K-13) is in shallow water.

At Fulmar we have been able to obtain wave directional information from the

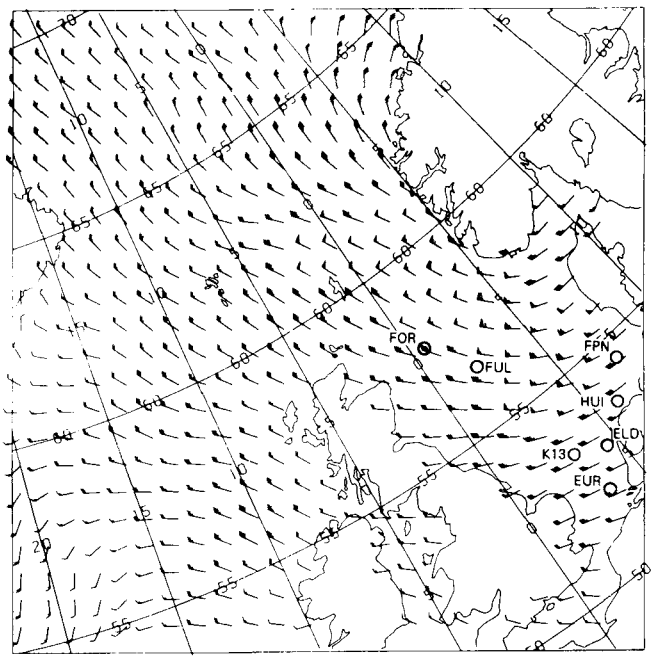


Figure 11. An example of the numerically reconstructed wind fields, on 12 GMT 24 November 1981. Also shown are the locations of the seven measurement stations. (FOR: Forties; FUL: Fulmar; HUI: Huibert: EUR: Euro)

Fulmar Wave Crest Kinematics (FULWACK) experiment (G. Z. Forristall, personal communication). By measuring the wave height, together with the two components of horizontal velocity using electromagnetic current meters, it is possible to derive the mean wave direction and directional spread (not used in this study) at each frequency, as described by Forristall *et al.* (1978).

At K-13 we have used waverider buoy measurements which were made some distance from the platform so that there is little influence of the platform on the wave field.

The significant wave height, $H_s$, and mean period, $T_{M01}$, were computed from the one-dimensional wave spectrum $F(f)$ using the relations $H_s = 4m_0^{1/2}$: $T_{M01} = m_0/m_1$ where the moments of the spectrum are determined from $m_n = \int_{0.05}^{0.5} f^n F(f)\,df$, with frequency $f$ in Hz.

Confidence limits for significant wave height and mean wave direction depend on the degrees of freedom of the spectral estimates (Long 1980). At Fulmar we estimate the 90% confidence limits for $H_s$ to be 1·05 and 0·95 times the expected value of $H_s$; at K-13 the corresponding values are 1·07 and 0·93. From the analysis at Fulmar we obtain ±6° as the 90% confidence interval for the mean wave direction. The 90% confidence limits for the wave energy spectra are 1·25 and 0·76 at Fulmar and 1·38 and 0·65 at K-13.

### (*e*) *The operational characteristics of the models*

The mathematical and physical bases of the three wave models have been described earlier in this paper. We now consider the operational characteristics of the models, that is their physical extents, resolution, boundary treatments, etc. The grid networks of the models are shown in Fig. 12 and the spatial resolutions given in Table 2. Apart from the obvious differences in resolution, the models have a major difference in the geographical area covered by the grids. The areas of the BMO and HYPAS models are very similar but that of GONO has a much greater northerly extent. This difference in area is largely negated in our study since the hindcast wind fields, prepared for the comparison runs, cover an area only slightly greater in extent than that of the BMO wave model grid. A zero wind field was specified in the GONO model for the areas north of that for which hindcast wind values were obtained; thus the possible effects of extra northerly fetch were avoided. The truncation of wind fields at the northern edge of the models is an obvious limitation to the extent to which the models can represent distantly generated swell. Such a situation did arise in the real hindcast experiment which is discussed later.

An associated problem with the wind field is the height to which the wind data can be attributed. Both GONO and HYPAS are formulated to use wind fields specified at a height of 10 m. The BMO model on the other hand is formulated to accept winds at a height of 19·5 m. As mentioned earlier (section 4(*c*)) the resultant wind fields of the

TABLE 2. PHYSICAL CHARACTERISTICS OF THE WAVE MODELS

| Characteristic | BMO | GONO | HYPAS |
|---|---|---|---|
| Spatial resolution (km) | 25 | 75 | 50 |
| Time step (minutes) | 30 | 90 | 30 |
| Directional resolution (°) | 22½ | 30 | 15 |
| Lowest frequency (Hz) | 0·04 | 0·05 | 0·0425 |
| Open boundary specification | Zero energy flux | Constant energy flux | Zero energy flux |

For swell the directional resolution in GONO is effectively higher than the 30° quoted. This is because within each directional sector of 30° the mean direction is also computed with a typical accuracy of 1°.

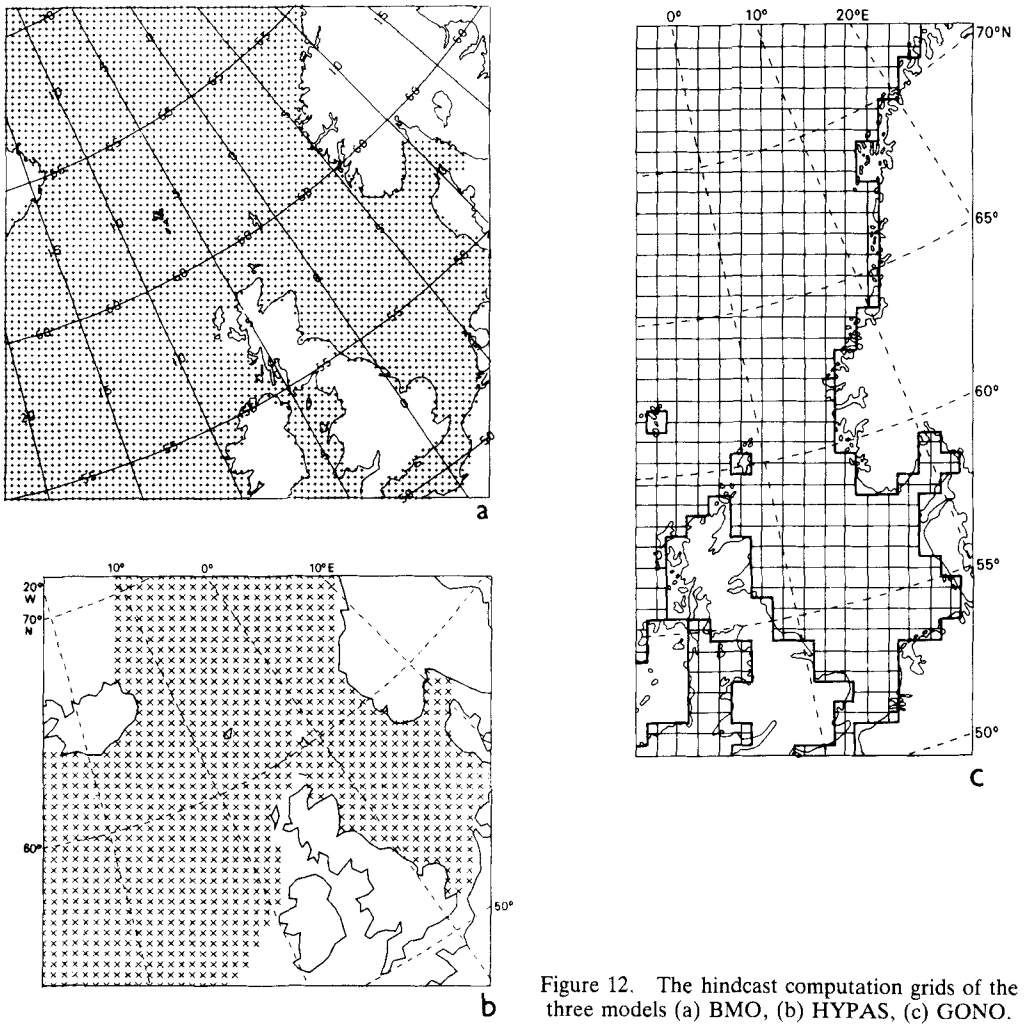


Figure 12. The hindcast computation grids of the three models (a) BMO, (b) HYPAS, (c) GONO.

analysis process are nominally valid for a height of 19·5 m. The degree of accuracy that can be ascribed to these wind fields is, however, wide enough to encompass the expected variation in speed and direction between the 10 m and 20 m levels. A wide range of boundary layer stability states was encountered during the period of the hindcast event, ensuring an appreciable scatter in the degree of accuracy to which winds at a specified level could be calculated. Accordingly no action was taken to adjust the wind fields to the 10 m level required by the GONO and HYPAS models. Such action would have required the use of further modelling assumptions, not necessarily increasing the expected accuracy of the wind field values.

The grid point values of sea depth were unique to each model, but differed only in minor detail due to grid resolution and coast line representation. An example of the typical somewhat smoothed topography, that of the BMO model, is shown in Fig. 13. Major features are adequately represented, for example the shallows associated with the northern islands and the complicated structure of the central and southern North Sea. None of the models have a spatial resolution adequate to resolve the more local features, such as sand banks, which characterize some parts of the southern North Sea.

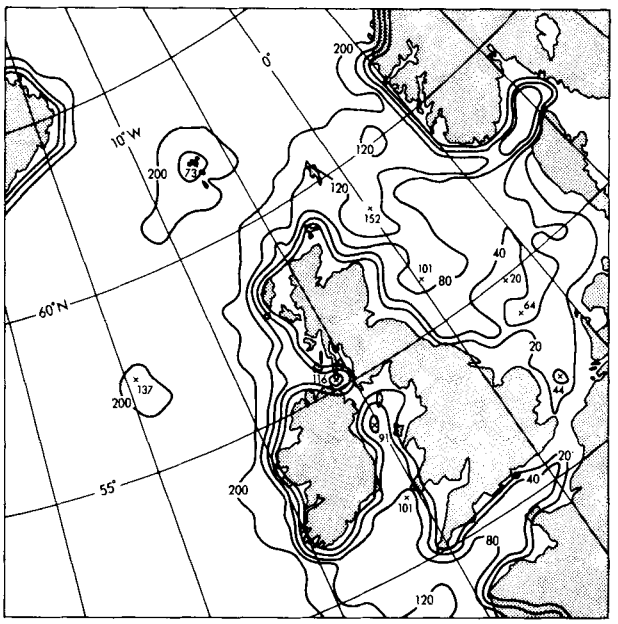


Figure 13: A typical example (BMO model) of the smoothed bottom topography included in the models. Contours of sea depth are in metres.

### (*f*) *Some results of the model hindcasts*

The two stations chosen for a detailed comparison exercise are each representative of very different geophysical situations. The northern station, Fulmar, is in deep water and during the study period experienced wind speeds of up to $30\,m\,s^{-1}$. Much of the energy in the associated wave fields was thus directly due to the local wind input. The directional wave information obtained during the study period adds a revealing extra dimension to the discussion of the performance of the three models. The southern station, K-13, is in much shallower water with an associated increased complexity in the bottom topography. The wind speeds measured in the south were lower ($\sim 20\,m\,s^{-1}$), but a large swell component from the north contributed to the total significant wave height and is apparent in the measured spectra.

The first station for which we consider results in detail is Fulmar. Measured wave data are not available for the complete period 20–26 November, but the peaks of both storms contained in that period were fortunately measured. Figure 14 shows time series plots of both $H_s$ and $T_{M01}$ for measurements and the results of all three models. The maximum observed values of $H_s$ were 8·1 m on the 20th and 11·1 m on the 24th. For the first storm only the GONO model attained a comparable peak height, both the HYPAS and BMO models failing to match the observed rapid growth in height between 15 z and 18 z on the 20th. The GONO model, although more successful in matching the observed maximum, had shown excessive growth early on in the day.

A similar pattern of behaviour occurred for the second storm event where once again only the GONO model gave a result comparable to the measured maximum value. All the models reached their peak values later than in reality, and the GONO and HYPAS models were too high during the entire decay phase. The behaviour of the models in terms of the period $T_{M01}$ was much closer, all had too low a peak value in the first storm (measured as 10·0 s) and all made a more reasonable match for the second

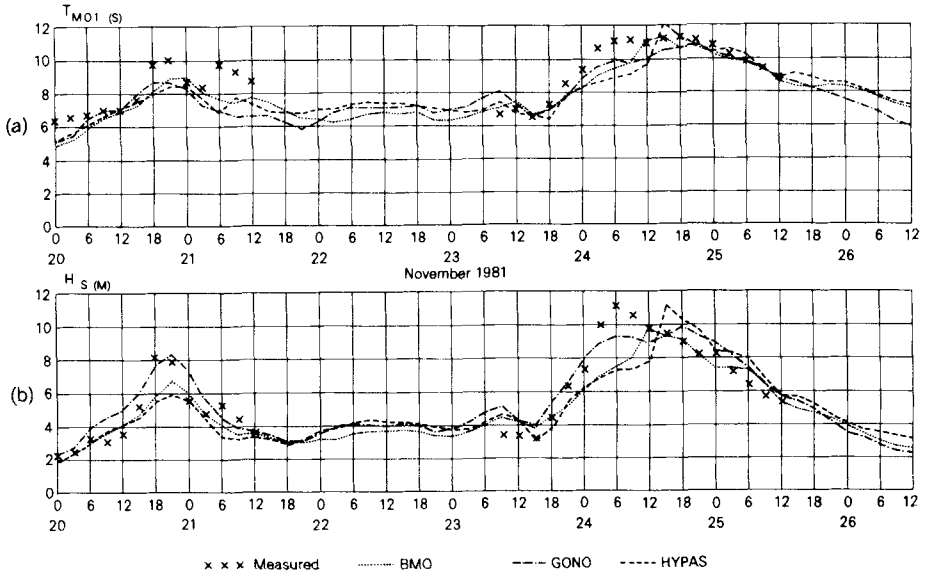


Figure 14. Timeseries plots of: (a) Mean zero-upcrossing period $T_{M01}$(seconds); (b) significant wave height $H_s$(metres); for location Fulmar during the hindcast period 20–26 November 1981. Results from the three models are intercompared and verified against measured data.

storm peak period (measured as 11·3 s) showing slow growth rates and reasonable decay rates.

The behaviour of the models in the first storm can be further analysed by means of the spectral plots shown in Fig. 15. In the early hours of the 20th low-frequency energy

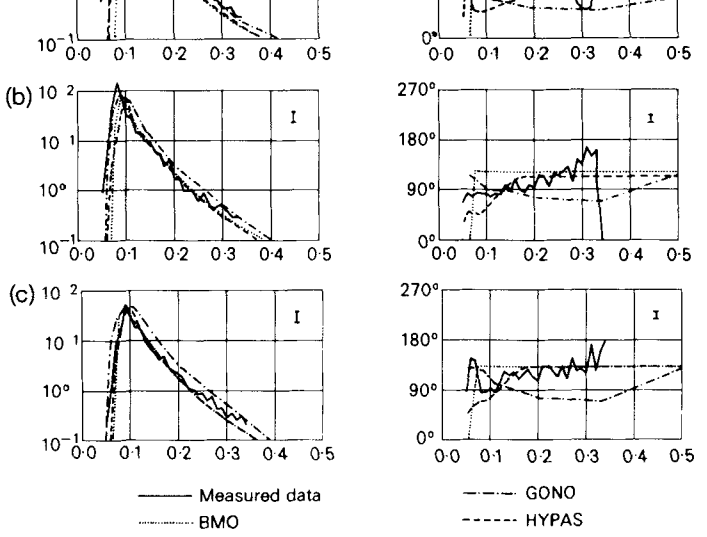


Figure 15. (a) 18 GMT, (b) 21 GMT 20 November, (c) 00 GMT 21 November 1981: logarithmic plots of wave energy against frequency (Hz) and plots of mean wave direction against frequency for location Fulmar. Results from the three models are intercompared and verified against measured spectra with 90% confidence limits shown in top right of each plot.

was arriving from the north, as seen in the observed data but not shown here. This energy was not reproduced in any of the models and was probably generated outside the model grids. The gradually rising wind-sea had obscured this swell component by 18 z, at which time the storm was at its peak. The controlled experiments in section 3(*a*) have revealed that the GONO model has a much more rapid growth rate than the others, so that in a duration-limit state such as the first storm at Fulmar (very rapid rise and fall in wind speed, see Fig. 9), it is not surprising that the GONO model achieved a higher energy level at the peak of the wind-sea (Fig. 15(a) for 18 z).

The continuing high levels of energy in the GONO model (21 z and 00 z for the 21st) are seen to be mostly due to an overestimate of the high-frequency flank of the spectrum. This feature is due to the way in which the GONO model reacts to a rapidly changing wind direction. As can be seen from Figs. 9 and 15 there was a change in wind direction at Fulmar of about 50° in the three hours 18 to 21 z. It can be seen that the BMO model relaxes completely in that time to the new wind direction even to the extent of an over-relaxation at the lower frequencies; the HYPAS model has adjusted over a more reasonable range (>0·1 Hz), whereas the GONO model is only coincident with the new direction (at 21 z) at the extreme plotted frequency of 0·5 Hz. The GONO model then treats part of the previous wind-sea as swell, since the remainder is no longer in the same direction as the wind, and effectively moves it to higher frequencies.

During the growth period of the second storm it was again apparent that all the models were lacking in the low-frequency energy that was visible in the measurements, coming from the north-west. The GONO model had higher energy levels than the other models due to a higher effective directional resolution in the discrete part of the spectrum, thus enabling a better estimate of the energy propagation from a source which even in reality is shaded by the coastlines of Scotland and its off-shore islands. An additional source of error was due to small inaccuracies in the hindcast wind field. An extensive manual analysis of the meteorological conditions (Caudwell and Draper 1984) has since revealed that actual and modelled winds in the early hours of the 24th differed by up to 2·5 m s$^{-1}$ in speed and 20° in direction. The direction error was of the greatest effect, giving shorter fetch westerly winds rather than the actual north-westerlies of longer fetch. As a result all the models reached their peak values late, and with lower energy values than those observed.

The overall statistics for the models, i.e. comparisons between measured and hindcast periods, are shown in Table 3. The predominant overestimate of the GONO model is clearly seen, in contrast with the underestimates of the other models. The statistics for the periods show the general accord between the models that is also apparent from the time series.

For the other station to be discussed, K-13, there are measurements available throughout the entire six-day period. The significant wave heights recorded were lower than at the northern station (5·7 m maximum on the 25th, a mean overall of 3·3 m) but since the depth at the station is 28 m it is readily apparent that shallow water processes played a much more significant role here than at Fulmar. The wind speeds at this station were lower than at Fulmar, with predominantly westerly elements in the wind direction implying limited fetch on most occasions.

The time series of significant wave height and $T_{M01}$ period (Fig. 16) show that overall energy levels between the models exhibited fewer differences at this southern station. The GONO model overestimated $H_s$ throughout most of the period but made a good estimate of energy levels during the peak of the 2nd storm, on the 25th. The HYPAS and BMO models have lower, more realistic, levels through the period, although the BMO model failed to match the higher energy levels of the 2nd storm. Periods were

TABLE 3. VERIFICATION STATISTICS FOR TWO NORTH SEA LOCATIONS, 20–26 NOVEMBER 1981

| Location | $N$<br>$\overline{H}_s$(m)<br>$\overline{T}_{M01}$(s) | Model | Model depth (m) | Mean height error (m) | r.m.s. height error (m) | Scatter index | No. of +ive errors | No. of −ive errors | Mean period error (s) | r.m.s. period error (s) | Scatter index | No. of +ive errors | No. of −ive errors |
|---|---|---|---|---|---|---|---|---|---|---|---|---|---|
| FULMAR | 31 | BMO | 82 | −0·4 | 1·1 | 19 | 11 | 20 | −0·6 | 0·7 | 8 | 8 | 23 |
| | 6·1 | GONO | 80 | +0·4 | 0·9 | 14 | 23 | 8 | −0·7 | 0·9 | 10 | 4 | 27 |
| | 9·0 | HYPAS | 75 | −0·4 | 1·5 | 24 | 12 | 19 | −0·7 | 0·9 | 10 | 7 | 24 |
| K-13 | 50 | BMO | 27 | −0·2 | 0·4 | 13 | 19 | 31 | −0·2 | 0·6 | 9 | 20 | 30 |
| | 3·3 | GONO | 25 | +0·4 | 0·5 | 14 | 40 | 10 | −0·1 | 0·7 | 10 | 21 | 29 |
| | 6·6 | HYPAS | 31 | −0·1 | 0·5 | 16 | 26 | 24 | −0·3 | 0·7 | 10 | 19 | 31 |

$N$ denotes number of observations
$\overline{H}_s$ denotes mean of observed significant wave heights
$\overline{T}_{01}$ denotes mean of observed periods
Scatter index = 100 × (r.m.s. error)/(mean obs.)

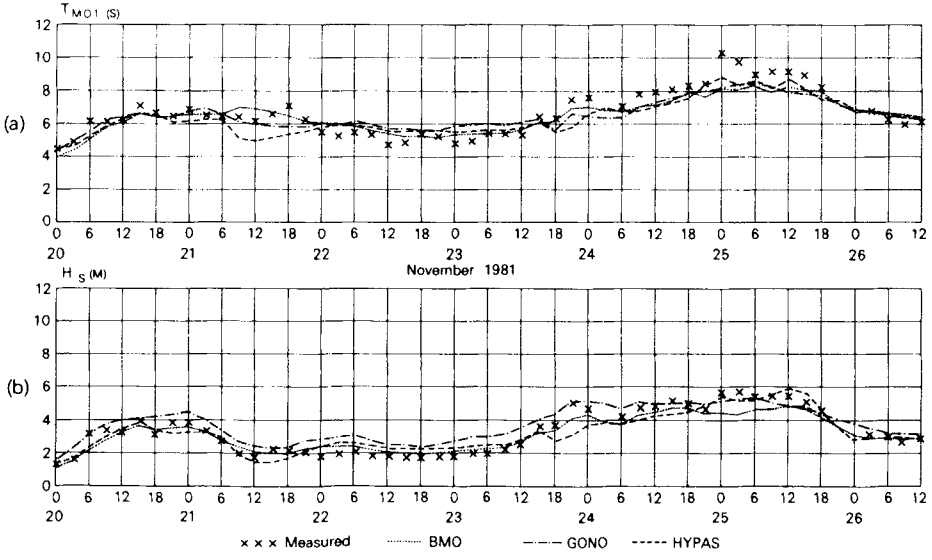


Figure 16. As Fig. 14 for location K-13.

generally well represented except for that of 00z on the 25th. This long period value (10·2 s) was probably due to the same low-frequency energy, visible in the observations but absent in the models, referred to earlier in the discussion of the Fulmar results and taking 12–24 hours to travel south. The summary statistics for K-13 can be seen in Table 3. Again, the overestimates of the GONO model are evident, but there is much less difference in the performance of the three models at this location than at Fulmar.

Two interesting spectral cases can be discussed, one of which is illustrated in Fig. 17. As mentioned above, the GONO model had too high an energy level throughout the period. The limited fetches, associated with predominantly westerly wind directions, were probably the cause of this since it is known from the results of section 3(*a*) that the GONO model has a higher growth rate than the other models in short fetch conditions and over-develops the wind-sea. The spectral plots for 03–09z on the 23rd (Fig. 17) illustrate this effect very nicely; the exaggerated wind-sea in the GONO model also hid the low-frequency swell features so well represented in the other models. For short fetches with wind speeds below 25 m s$^{-1}$ all of the models treat the development of wind-sea as being effectively a deep water case.

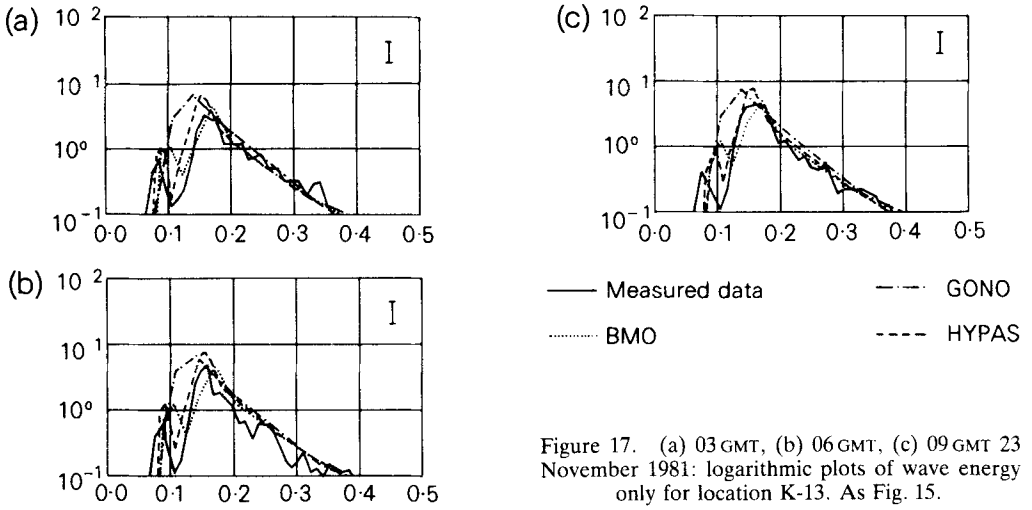


Figure 17. (a) 03 GMT, (b) 06 GMT, (c) 09 GMT 23 November 1981: logarithmic plots of wave energy only for location K-13. As Fig. 15.

The second spectral case worth discussion centres on the performance of the BMO model in the early hours of the 25th. As can be seen from the time series in Fig. 16 the values of $H_s$ were much too low at that time. This effect may be explained as a result of the too rapid adjustment of the spectrum to wind direction changes, already discussed in the Fulmar results. Energy from the north that should have arrived at K-13 as swell, and which was evident in both observed spectra and the results of the other models, was instead turned with the tightly curving wind field present in the mid North Sea on the 24th and propagated eastwards. This diagnosis was confirmed by an examination of results for another data source off the Danish coast where energy levels were far too high in the BMO hindcast for the 25th.

## 5. Conclusions

The aim of the authors of this paper was primarily to test their respective wave models in shallow water situations, in order to gain some insight into the effects of the different parametrization of the physical processes involved. The three models considered have some similarities, but many more differences, hence it was assumed that in a

hindcast situation the performances of the models would differ considerably and that detailed analyses would be able to diagnose causes and effects in terms of the different model physics.

To further this aim we first carried out the 'controlled' experiments of section 3, and were able to interpret clearly the different results of the models in a diagnostic manner, relating the differing evolutions and equilibrium states to the underlying physical assumptions and their mathematical solutions.

The particular hindcast real storm event was chosen for the reasons outlined earlier, rather than after a careful selection procedure. However, from the difficulty experienced in interpreting the results of a real hindcast in terms of model characteristics, it is perhaps doubtful that a more carefully selected storm would have yielded more helpful information. The clear aspects of model performance which emerged from the hindcast study are as follows:

(a) All the models successfully reproduced the various levels of wave energy evident in the course of the real storm. Maximum and minimum energy levels in high and low wind speed regimes were acceptably reproduced and the obvious shallow water reduction of energy at the southern locations was also successfully achieved.

(b) Some spectral features were correctly modelled, including the growth of wind-sea and the presence of swell as a separate component of the spectrum.

(c) The directional information at Fulmar confirmed earlier impressions that the modelling of rapidly turning wind fields needs further study. The BMO model requires an alternative to the rapid adjustment mechanism, which is insensitive to the different relaxation rates required at different frequencies. The GONO model also revealed interpretation problems associated with turning wind-sea and swell.

(d) Various shortcomings of all the models were revealed: excessive growth rates in fetch- and duration-limited situations (GONO); an overall negative bias of energy levels (HYPAS and BMO).

The one other very important general fact that emerged from the hindcast study was the virtual impossibility of separating out the effects of various modelling processes. Although the models are based on different theoretical spectra they all generally managed to assess correctly the wind-sea; although having different assumptions about dissipation they all generally assessed the correct total energy levels. The detailed balances between individual processes were, however, sufficiently obscured by the interaction of all the physical influences on wave generation that the intended analytical study became difficult to carry out.

Any further attempt to compare wave models in real physical situations must set itself more limited aims, and be capable of more control over the measurement of the physical data. As said earlier even a more careful selection of a storm event might not have yielded more insight into model performance, since it is now apparent that a purpose-designed network of wave observations is also required if meaningful diagnosis of the separate physical processes is going to be attempted.

The success of the respective models, in hindcast mode, in representing the general features of the real wave fields cannot, however, be over-emphasized. Wave models, especially if they can be improved by the removal of weaknesses highlighted in this paper, now offer a real means of establishing 'climatology' for use in many practical applications.

## APPENDIX

*The derivation of the energy density balance equation, in frequency direction space, from the action density balance equation in wavenumber space.*

We begin with the action density balance equation in wavenumber space

$$\partial N/\partial t + \mathbf{c}_g \cdot (\partial N/\partial \mathbf{x}) - (\partial \omega/\partial \mathbf{x}) \cdot (\partial N/\partial \mathbf{k}) = S \tag{A1}$$

where $N = N(\mathbf{k}, \mathbf{x}, t)$ is the action density; $\mathbf{c}_g = \partial \omega/\partial \mathbf{k}$ is the group velocity.

The transformation to energy density $F(\mathbf{k}, \mathbf{x}, t)$ is straightforward since $F = \omega N$.

$$\partial F/\partial t + \mathbf{c}_g \cdot (\partial F/\partial \mathbf{x}) - (\partial \omega/\partial \mathbf{x}) \cdot (\partial F/\partial \mathbf{k}) = \omega S, \tag{A2}$$

since $\omega \neq \omega(t)$. The next transformation is that from wavenumber space into frequency–direction space. If $G(\mathbf{k})$ and $G'(\omega, \theta)$ are the respective functions in these spaces then the relationship between them is given by

$$G(\mathbf{k}) = G'(\omega, \theta)(c_g/k) \quad \text{where} \quad c_g = |\partial \omega/\partial \mathbf{k}| \quad \text{and} \quad k = |\mathbf{k}|. \tag{A3}$$

Care has to be taken to preserve the partial differentials of Eq. (A2); consequently use is made of the dispersion relationship

$$\omega^2 = gk \tanh kH \tag{A4}$$

in order to progress to

$$\frac{\partial F}{\partial t} + \frac{\partial}{\partial \mathbf{x}}(\mathbf{c}_g F) + R\left\{F\mathbf{c}_g \cdot \frac{\partial H}{\partial \mathbf{x}} - kc_g \frac{\partial H}{\partial \mathbf{x}} \cdot \frac{\partial \theta}{\partial \mathbf{k}} \frac{\partial F}{\partial \theta}\right\} = \omega S \tag{A5}$$

where $F$ and $S$ are now in frequency–direction space, and

$$R = k(kH + \sinh kH \cosh kH)^{-1}.$$

It is easily shown that

$$\mathbf{c}_g \cdot \frac{\partial H}{\partial \mathbf{x}} = c_g \left\{\frac{\partial H}{\partial x}\cos\theta + \frac{\partial H}{\partial y}\sin\theta\right\} = -\frac{\partial}{\partial \theta}\left|\mathbf{c}_g \Lambda \frac{\partial H}{\partial \mathbf{x}}\right|$$

and that

$$kc_g \frac{\partial H}{\partial \mathbf{x}} \cdot \frac{\partial \theta}{\partial \mathbf{k}} = c_g \left\{-\frac{\partial H}{\partial x}\sin\theta + \frac{\partial H}{\partial y}\cos\theta\right\} = \left|\mathbf{c}_g \Lambda \frac{\partial H}{\partial \mathbf{x}}\right|$$

hence (A5) becomes

$$\frac{\partial F}{\partial t} + \frac{\partial}{\partial \mathbf{x}}(\mathbf{c}_g F) - \frac{\partial}{\partial \theta}\left\{RF\left|\mathbf{c}_g \Lambda \frac{\partial H}{\partial \mathbf{x}}\right|\right\} = \omega S \tag{A6}$$

which is the required result.

## ACKNOWLEDGMENTS

We thank the Shell Development Company, Houston, and the Rijkswaterstaat for supplying measured wave data in the North Sea.

## REFERENCES

Bouws, E. and Komen, G. J. 1983 On the balance between growth and dissipation in an extreme depth-limited wind-sea in the southern North Sea. *J. Phys. Ocean.*, **13,** 1653–1658

Bouws, E., Gunther, H., Rosenthal, W. and Vincent, C. L. 1985a Similarity of the wind wave spectrum in finite depth water, Part I—Spectral form. *J. Geophys. Res.*, **90**, 975–986

Bouws, E., Komen, G. J., van Moerkerken, R. A., Peeck, H. H. and Saraber, M. J. M. 1985b 'An evaluation of operational wave forecasts on shallow water'. Proc. IUCRM Symposium on Wave Dynamics and Radio Probing of the Ocean Surface, Miami, Plenum Press

Bretschneider, L. 1958 'Revisions in wave forecasting: deep and shallow water'. Proc. 6th Conf. on Coastal Eng., Ch. 3, pp 30–67

Burridge, D. M. and Gadd, A. J. 1977 'The Meteorological Office operational 10-level numerical weather prediction model (December 1975)'. Met. O. Sci. Pap. 34. HMSO, London

Caudwell, W. D. and Draper, L. 1984 'Case Study of the North Sea Storm of 23/24 November 1981'. Unpublished report, Dept. of Energy PET 74/1125/45

Collins, J. I. 1972 Prediction of shallow water spectra. *J. Geophys. Res.*, **77,** 2693–2707

Findlater, J., Harrower, T. N. S., Hawkins, G. A and Wright, H. L. 1966 'Surface and 900 mb wind relationships'. Met. O. Sci. Pap. 23, HMSO, London

Forristall, G. Z., Ward, E. G., Cardone, V. J. and Borgmann, L. E. 1978 The directional spectra and kinematics of surface gravity waves in tropical storm Delia. *J. Phys. Ocean.*, **8,** 888–909

Golding, B. W. 1983 A wave prediction system for real time sea state forecasting. *Quart. J. R. Met. Soc.*, **109,** 393–416

Gunther, H., Rosenthal, W., Weare, T. J., Worthington, B. A., Hasselmann, K. and Ewing, J. A. 1979 A hybrid parametrical wave prediction model. *J. Geophys. Res.*, **84**, 5727–5738

Gunther, H. and Rosenthal, W. 1984 'A shallow water surface wave model based on the TEXEL-MARSEN-ARSLOE (TMA) wave spectrum'. Proc. 20th Congress IAHR, Moscow, 1983

Gunther, H., Rosenthal, W. and Komen, G. J. 1984 A semi-operational comparison of two parametrical wave prediction models. *Deut. Hydrogr. Z.*, **37,** 89–106

Hasselmann, K., Barnett, T. P., Bouws, E., Carlson, H., Cartwright, D. E., Enke, K., Ewing, J. A., Gienapp, H., Hasselmann, D. E., Kruseman, P., Meerburg, A., Muller, P., Olbers, D. J., Richter, K., Sell, W. and Walden, H. 1973 Measurements of wind-wave growth and swell decay during the Joint North Sea Wave Project (JONSWAP). *Deut. Hydrogr. Z.* A12

Holthuijsen, L. H. 1980 *Methoden voor Golfvoorspelling.* Technische Afviescommissie voor de Waterkeringen, The Hague, 2 vols.

Janssen, P. A. E. M., Komen, G. J. and de Voogt, W. J. P. 1984 An operational coupled hybrid wave prediction model. *J. Geophys. Res.*, **89,** (C3), 3635–3654

Kitaigorodskii, S. A., Krasitskii, V. P. and Zaslavskii, M. M. 1975 On Phillips theory of equilibrium range in the spectra of wind-generated gravity waves. *J. Phys. Ocean.*, **5,** 410–420

Komen, G. J., Hasselmann, S. and Hasselmann, K. 1984 On the existence of a fully developed wind-sea spectrum. *ibid.*, **14,** 1271–1285

Long, R. B. 1980 The statistical evaluation of directional spectral estimates derived from pitch-roll buoy data. *ibid.*, **10,** 944–952

Shemdin, O., Hasselmann, K., Hsiao, S. V. and Herterich, K. 1978 'Non-linear and linear bottom interaction effects in shallow water', in *Turbulent fluxes through the sea surface, wave dynamics and prediction.* Ed. A. Favre and K. Hasselmann, Plenum Press, pp. 629–645

SWAMP group: Allender, J. H., Barnett, T. P., Bertotti, L., Bruinsma, J., Cardone, V. J., Cavaleri, L., Ephraums, J. J., Golding, B., Greenwood, A., Guddal, J., Gunther, H., Hasselmann, K., Hasselmann, S., Joseph, P., Kawai, S., Komen, G. J., Lawson, L., Linne, H., Long, R. B., Lybanon, M., Maeland, E., Rosenthal, W., Toba, Y., Uji, T., de Voogt, W. J. P.

1982 'Sea Wave Modelling Project (SWAMP): An intercomparison study of wind-wave prediction models, Part 2—A compilation of results'. KNMI Pub. 161

1985 'Sea Wave Modelling Project (SWAMP): An intercomparison study of wind-wave prediction models, Part 1—Principle results and conclusions'. Proc. IUCRM Symp. on Wave Dynamics and Radio Probing of the Ocean Surface, Miami, Plenum Press

Vincent, C. L. 1982 'Shallow water wave modelling'. Proc. 1st. Int. Conf. on Meteorology and Air–sea Interactions in the Coastal Zone. The Hague, Amer. Met. Soc., 87–95